



Viscosity of slags from joint smelting of oxidized nickel and sulfide copper ores

Alexander KLYUSHNIKOV¹, Svetlana SERGEEVA¹, Roza GULYAEVA¹,
Alexander VUSIKHIS¹, Lyudmila UDOEVA², Stanislav TYUSHNYAKOV¹

1. Laboratory of Non-Ferrous Metals Pyrometallurgy, Department of Non-Ferrous Metals, Institute of Metallurgy of the Ural Branch of the Russian Academy of Sciences, 101, Amundsen Street, Yekaterinburg 620016, Russia;
2. Laboratory of Rare Refractory Metals, Department of Non-Ferrous Metals, Institute of Metallurgy of the Ural Branch of the Russian Academy of Sciences, 101, Amundsen Street, Yekaterinburg 620016, Russia

Received 22 July 2022; accepted 12 April 2023

Abstract: The work is devoted to the viscosity determination of molten slags from the joint smelting of oxidized nickel and sulfide copper ores. The model slags were synthesized close in composition and structure to real samples, and limiting the investigated composition range (wt.%): iron-containing slag (8.9 CaO, 11.8 MgO, 12.5 Al₂O₃, 47.4 SiO₂, 13.3 FeO, and 5.0 Fe₂O₃) and iron-free slag formed by removing iron oxides from the iron-containing slag (12.5 CaO, 16.0 MgO, 9.4 Al₂O₃, and 58.3 SiO₂). The experimental (vibrational method) viscosity values for iron-containing (1550–1300 °C) and iron-free (1550–1400 °C) model slags are 0.31–2.33 and 1.28–4.55 Pa·s, respectively. Viscosity estimation by the Kalmanovitch–Frank model shows a discrepancy with the experimental data for iron-containing slag. Regression analysis (by Weimann–Frenkel–Urbain formalism) of the experimental data was carried out, and original empirical models were proposed to predict the primary model slags viscosity in the considered temperature range. Reducing the basicity from 0.7 (iron-containing slag) to 0.6 (iron-free slag) increases viscous flow activation energy from 204 to 236 kJ/mol. To maintain optimal slag viscosity, joint smelting of oxidized nickel and sulfide copper ores should be carried out at a temperature not lower than 1400 °C.

Key words: slag; viscosity; vibrational viscometer; Kalmanovitch–Frank model; Weimann–Frenkel–Urbain equation; oxidized nickel ore; sulfide copper ore; matte smelting

1 Introduction

The depletion of reserves and the increasing complexity of the composition of mineral raw materials used in nickel and copper production make it necessary to search for technologies that ensure the maximum utilization degree of all valuable components of ores. A promising approach to solving this problem is direct joint pyrometallurgical processing of sulfide and oxide

raw materials. The advantages of this approach are described in Refs. [1–7]. Previously, the authors of this work have studied the possibility of concentrating nickel, copper, and cobalt in sulfide–metallic melts (mattes) during laboratory smelting (1300–1500 °C) of mixtures of oxidized nickel and sulfide copper ores from deposits of the Ural region (Russia), flux (calcium oxide), and the reducing agent (graphite or coke) in an inert or weakly reducing gas atmosphere. For matte enrichment in a number of experiments, the copper

ore was previously subjected to partial oxidative roasting in the air with the removal of about 75% of sulfur into the gas phase (the chemical compositions of the ores and flux are presented in Table 1) [2,8]. The investigation was aimed at increasing the useful specific capacity of the furnace and reducing SO₂ emission during smelting by reducing flux consumption, increasing the degree of matte metallization, and using copper ore sulfur for sulfiding non-ferrous metal oxide forms. A number of mixtures of oxidized nickel ore, sulfide copper ore (or calcine), calcium oxide, and graphite were melted, taken in a mass ratio of 100:(10–60):10:(1–5). The smallest losses of non-ferrous metals were noted in slags containing 50–61 wt.% SiO₂, 1–16 wt.% Fe_{total}, 14–17 wt.% MgO, 4–5 wt.% Al₂O₃, 9–12 wt.% CaO, and 0.2–0.8 wt.% S. This is consistent with the known data on the reduction of electrochemical and mechanical losses of non-ferrous metals with acidic slags [9]. It was found that increased consumption of the carbon-reducing agent during smelting led to increased matte metallization and transition from iron-containing (~16 wt.% Fe_{total}) to iron-free (<1 wt.% Fe_{total}) slag. Such transition was accompanied by a decrease in the contents of nickel, copper, and cobalt in oxide melt from 0.09, 0.12, and 0.02 to 0.01, 0.02, and 0.01 wt.%, respectively.

For further development of the technology of joint ore processing, information on the viscosity of such melts, primarily on the effect of temperature and changes in composition due to the removal of iron oxides from them, is needed. To date, a significant amount of experimental data on the

viscosity of melts of the CaO–MgO–FeO_x–Al₂O₃–SiO₂ system and its subsystems has been accumulated [10–44]. Direct distribution of these data on specific objects is complicated by differences in the chemical composition of the latter from the composition of previously studied materials, uncertainties inherent in the methods used, etc. There are a lot of calculation models for predicting the viscosity of slag by chemical composition and temperature [18,25,34,45–54], but the possibilities of their application are limited by narrow ranges of variation of the considered parameters and considerable estimation error [18,24,46]. Thus, the viscosity determination of slag is an urgent and non-trivial task. Its solution can contribute to the development of scientific ideas about the properties of the CaO–MgO–FeO_x–Al₂O₃–SiO₂ system, which plays an important role in geology, non-ferrous and ferrous metallurgy, glass making, and ceramics production, coal gasification, etc.

In this regard, the present work is devoted to the viscosity determination of molten slags from the joint smelting of oxidized nickel and sulfide copper ores. For this purpose, model slags were synthesized that are close to real prototypes in the content of the main components and structure, theoretical viscosity evaluation and experimental viscosity measurement of model samples were carried out, original empirical models describing temperature changes of viscosity were formulated and verified, and regularities of viscosity changes related to the removal of iron oxides from the slag were studied.

Table 1 Chemical compositions of oxidized nickel and sulfide copper ores, flux and slags from smelting their mixtures (according to X-ray fluorescence analysis)

Material	Content/wt.%										
	Ni	Cu	Co	Zn	Fe _{total}	S	SiO ₂	MgO	Al ₂ O ₃	CaO	Others
ONO	1.16	–	0.06	–	8.1	–	52.6	13.6	5.1	1.0	18.3
SCO	0.01	1.10	0.14	1.30	35.7	31.0	13.0	5.5	1.2	1.2	9.9
Calcine	0.01	1.45	0.18	1.37	45.4	10.6	16.5	7.0	1.5	1.5	14.5
Flux	–	–	–	–	–	–	–	–	–	96.0	4.0
ICS	0.09	0.12	0.02	0.20	15.7	0.2	50.0	14.2	4.8	9.4	5.3
IFS	0.01	0.02	0.01	0.01	1.1	0.8	60.7	17.4	5.4	12.3	2.2

ONO and SCO are oxidized nickel ore and sulfide copper ore, respectively; Calcine is a product of partial oxidative roasting of the sulfide copper ore (the particle size and moisture content of the ores are <0.1 mm and <1 wt.%, respectively); ICS and IFS are iron-containing and iron-free slags, respectively. Based on the data [9] on the properties of slags of reduction–sulfiding smelting of copper–nickel raw materials, it is assumed that all the iron in the slags is in the form of Fe²⁺, and sulfur is in the dissolved form as FeS

2 Experimental

2.1 Materials

In this work, model slag samples were used, similar in the content of the main components to their real prototypes (iron-containing (ICS) and iron-free (IFS) slags from Table 1). To simplify the task, non-ferrous metals were excluded from the composition of the prototypes (since sulfur in the slag exists in the form of dissolved anion S^{2-} , it was retained in its composition to take into account its possible influence on its properties), and the contents of other components were normalized. The following slag compositions (wt.%) were set: (1) 50.7 SiO₂, 20.0 FeO, 14.4 MgO, 9.5 CaO, 4.9 Al₂O₃, and 0.2 S (hereinafter designated as iron-containing primary model slag); (2) 61.9 SiO₂, 17.8 MgO, 12.6 CaO, 5.5 Al₂O₃, 1.4 Fe_{total}, and 0.8 S (hereinafter designated as iron-free primary model slag). Slight differences in the composition of model slags compared with prototypes are associated with the removal of “others” (except for oxygen associated with iron) from their composition and subsequent normalization.

The samples of primary model slags were synthesized from commercial high-purity chemical reagents (Table 2) at 1500 °C for 30 min. During the experiment, an inert gas (99.99 vol.% Ar) was continuously fed into the working zone of the furnace through the alumina tube at a flow rate of 50 cm³/min. The temperature was controlled with an error of ±5 °C using a TPP platinum–rhodium–platinum thermocouple; its hot junction, protected by an alumina case, was placed next to the crucible at the level of the melt mirror as close as possible to

its outer surface. After soaking, the furnace was cooled at room temperature (25 °C), and the slag was crushed and sent to study the material composition and viscosity measuring.

2.2 Characterization techniques

The elemental composition of samples of primary model slags was determined using chemical analysis (CA) methods. The phase composition of samples was measured by the X-ray powder diffraction (XRD) method using a DRON–2.0 X-ray diffractometer (Cu K_α radiation, the voltage and current on the tube are 30 kV and 40 mA, respectively). Phase identification in the crystal component of the samples was performed using the QualX 2.0 software [55] and the Pow_Cod database [55].

The microstructure and local elemental composition of the primary model slag samples were studied by scanning electron microscopy (SEM) and energy dispersive spectrometry (EDS) using a MIRA 3 LMU (TESCAN) auto emission electron microscope equipped with an INCA Energy 350 X-max 80 energy dispersive X-ray spectrometer (Oxford Instruments). The electronic sensing was performed at an accelerating voltage of 20 kV, an electron beam current of 20 nA, and an effective beam resolution of 3 μm. The sizes and volume fractions of mineral grains and glass in the sample were determined by SEM data using the planimetric method [56].

The value of the anion structure coefficient (ASC) of slags, equal to the ratio of the total number of oxygen atoms to the sum of the number of silicon atoms and taken with a coefficient of 0.75, the number of aluminum atoms of the sample

Table 2 Composition of charge for synthesis of primary model slags (per 100 g of slag)

Chemical reagent (Formula of active substance)	Active substance content/wt.%	Active substance mass/g		Chemical reagent mass/g	
		ICS	IFS	ICS	IFS
Silicon dioxide (SiO ₂)	98.00	50.66	61.94	51.69	63.20
Magnesium oxide (MgO)	98.00	14.39	17.75	14.68	18.12
Aluminum oxide (Al ₂ O ₃)	97.00	4.86	5.51	5.01	5.68
Calcium oxide (CaO)	97.50	9.52	12.55	9.77	12.87
Iron(III) oxide (Fe ₂ O ₃)	95.00	14.83	–	15.61	–
Carbonyl iron (Fe)	99.96	5.18	–	5.19	–
Natural pyrite (FeS)	73.28	0.56	2.24	0.76	3.05

The particle size and moisture content of the materials are <0.1 mm and <0.5 wt.%, respectively

(per 1 mol of the slag), was calculated by the formula [9]:

$$\text{ASC} = (2X_{\text{SiO}_2} + 3X_{\text{Al}_2\text{O}_3} + 3X_{\text{Fe}_2\text{O}_3} + X_{\text{MgO}} + X_{\text{CaO}} + X_{\text{FeO}}) / (X_{\text{SiO}_2} + 1.5X_{\text{Al}_2\text{O}_3}) \quad (1)$$

The value of the basicity modulus (B_{mol}) was determined by the expression:

$$B_{\text{mol}} = \frac{X_{\text{MgO}} + X_{\text{CaO}} + X_{\text{FeO}}}{X_{\text{SiO}_2} + X_{\text{Al}_2\text{O}_3}} \quad (2)$$

where X_{SiO_2} , $X_{\text{Al}_2\text{O}_3}$, $X_{\text{Fe}_2\text{O}_3}$, X_{MgO} , X_{CaO} , and X_{FeO} are the mole fractions of SiO_2 , Al_2O_3 , Fe_2O_3 , MgO , CaO , and FeO , respectively (for prototypes and synthesized model samples, contents of the element were taken from CA data; the compositions were converted to oxides and normalized during the calculation modeling).

The liquidus temperatures of the primary model slags were determined by differential scanning calorimetry (DSC) on an STA 449 C Jupiter[®] instrument (NETZSCH). The samples (19–20 mg) were placed in an alumina crucible, covered with an alumina lid with a calibrated hole, placed in the measuring cell of the instrument, and heated from 30 to 1450 °C at a rate of 20 °C/min with high-purity argon flow rate of 30 cm³/min. Processing of the measurement results with the determination of the extrapolated temperatures of the onset (T_o , °C), temperatures of the maxima ($T_{p,k}$, °C, where k is the maxima number) and extrapolated temperatures of the endset (T_e , °C) of the melting peaks was carried out using the Proteus program (NETZSCH). The separation of complex DSC peaks into their constituent overlapping elementary peaks and the determination of the refined temperatures of the elementary peak maxima ($T_{p,i}^r$, °C, where i is the number of the elementary peak) of the latter were carried out using the MathWorks software [57] according to the method described in Ref. [58]; the baseline was characterized by a linear function, the profile of elementary peaks was approximated by the Fraser–Suzuki function (asymmetric Gaussian function); the reliability of the approximation (for a significance level of $\alpha=5\%$) was controlled by the value of the Pearson correlation coefficient (r). The largest of the values $T_{p,i}^r$ was taken as estimates of the slag liquidus temperatures.

2.3 Viscosity calculation method

Theoretical viscosity (η , Pa·s) of slags in the temperature range of 1300–1550 °C was estimated using the Kalmanovitch–Frank model [34,53] (this model is a modification of the Urbain model [52], which is widely used to describe the viscosity of silicate systems due to the simplicity of calculations and the reliability of the results [34]). The formalism defined by the following equations [34] was used:

$$\eta_{\text{KFM}} = A_{\text{KFM}} T \exp\left(\frac{1000 B_{\text{KFM}}}{T}\right) \quad (3)$$

$$-\ln A_{\text{KFM}} = 0.2812 B_{\text{KFM}} + 14.1305 \quad (4)$$

$$B_{\text{KFM}} = B_0 + B_1 X_{\text{SiO}_2} + B_2 X_{\text{SiO}_2}^2 + B_3 X_{\text{SiO}_2}^3 \quad (5)$$

$$B_0 = 13.8 + 39.9355\alpha - 44.049\alpha^2 \quad (6)$$

$$B_1 = 30.481 - 117.1505\alpha + 129.9978\alpha^2 \quad (7)$$

$$B_2 = -40.9429 + 234.0486\alpha - 300.04\alpha^2 \quad (8)$$

$$B_3 = 60.7619 - 153.9276\alpha + 211.1616\alpha^2 \quad (9)$$

$$\alpha = \frac{X_{\text{CaO}} + X_{\text{MgO}} + X_{\text{FeO}}}{X_{\text{CaO}} + X_{\text{MgO}} + X_{\text{FeO}} + X_{\text{Al}_2\text{O}_3} + X_{\text{Fe}_2\text{O}_3}} \quad (10)$$

where η_{KFM} (Pa·s) is the calculated viscosity; A_{KFM} (Pa·s·K⁻¹), and B_0 , B_1 , B_2 , B_3 , B_{KFM} (K) are the model parameters. The calculation was based on the data on elemental composition (in mole fractions after normalization on the oxide amount) of the two primary model slags (iron-containing and iron-free) and four transitional model slags formed by the mental removal of 20%, 40%, 60%, and 80% of the initial amount of iron oxides from the iron-containing slag (that is, the formal iron oxides removal completeness (IRC, %), calculated as the ratio of the summary mass of all iron oxides mentally removed from the slag to their summary mass in the iron-containing primary model slag, of the six specified slags was changed from 0 to 100% in 20% steps). The compositions of intermediate slags were obtained by normalizing the amounts of components that remained after the removal of the appropriate amount of iron oxides from the iron-containing primary model slag.

2.4 Viscosity measurement method

Experimental estimation of the viscosity of molten primary model slag was carried out by

the vibrational method [59,60] under continuous cooling conditions. For this purpose, a laboratory setup was used, the design of which is described in Refs. [32,61–63]. Viscosity measurement limits on this setup are 0.01–20 Pa·s; the systematic error does not exceed $\pm 5\%$ [32,63]. The main elements of the setup (Fig. 1) are the measuring and melting modules.

Viscosity measurement was carried out as follows. A portion of the test sample (particle size

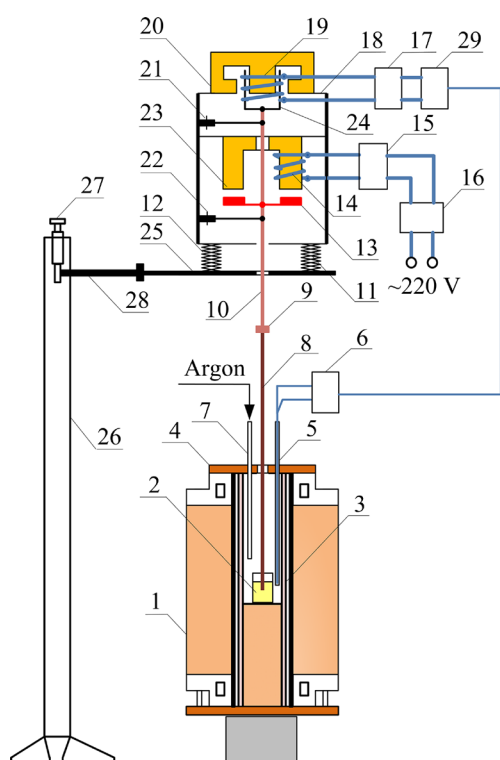


Fig. 1 Schematic of laboratory setup for measuring viscosity of molten slag (not to scale): 1–Electric resistance furnace (200 mm working zone height); 2–Molybdenum crucible (22 mm inner diameter, 50 mm height, 10 mm bottom and wall thickness) with molten slag; 3–Alumina cylinder (60 mm inner diameter, 500 mm height, 5 mm wall thickness); 4–Asbestos lid; 5–Thermocouple in an alumina case; 6–Millivoltmeter; 7–Alumina tube; 8–Molybdenum spindle (400 mm long and 1.5 mm diameter); 9–Clamp; 10–Brass rod (200 mm length and 5 mm diameter); 11, 12–Steel spiral springs; 13–Armature; 14–Excitation winding; 15–Autogenerator; 16–Voltage stabilizer; 17–Millivoltmeter; 18–Steel frame; 19–Winding of movable system; 20–Ring-type permanent magnet; 21, 22–Flat springs; 23–Package of plates made of transformer iron; 24–Frame of winding of movable system; 25–Shelf; 26–Support column; 27–Lifter with micrometer screw; 28–Rod; 29–Personal computer

less than 0.1 mm) weighing 30–40 g was poured into the molybdenum crucible (Item 2 in Fig. 1), and the crucible was placed into the working zone of the furnace (1), which ensured the uniformity of the temperature field. After that, the temperature in the working zone of the furnace was raised to 1550 °C with an average heating rate of 17 °C/min. The temperature was controlled with an error of ± 5 °C using a TPP platinum–rhodium–platinum thermocouple (5) and a millivoltmeter (6) calibrated for it; the hot junction of the thermocouple, protected by an alumina case, was placed next to the crucible as close as possible to its outer surface at the level of the melt mirror. An inert gas (99.99 vol.% Ar) was continuously fed into the working zone of the furnace through the alumina tube (7) at a flow rate of 50 cm³/min. Upon reaching 1550 °C, melting of the charge material was visually controlled, and isothermal soaking was carried out for 30 min, after which the voltage stabilizer (16) was connected to the alternating current network (voltage 220 V, frequency 50 Hz), while the mobile system began to make forced oscillations along the vertical axis with a frequency of about 17 Hz and an amplitude of 1 mm (the resonant oscillation mode was automatically maintained by the autogenerator (15)). Using the lifter with a micrometric screw (27), the spindle (8) was lowered into the melt to a depth of 10 mm (the moment the spindle touched the melt surface, corresponding to the zero point of immersion, was recorded using the millivoltmeter (17)). By adjusting the position of the rod (28), coaxiality was achieved in the arrangement of the spindle (8) and the crucible (2). After stabilization of the readings of the millivoltmeter (17), three consecutive cooling–heating cycles of the slag were carried out according to the scheme 1550 → 1300 → 1550 °C (the average heating and cooling rates were 17 and 5 °C/min, respectively). In the cooling stage, every 25 °C, using the millivoltmeter (17), a variable electromotive force (ε , V) was recorded in the winding of the movable system (19), which was proportional to the resonant frequency of the spindle oscillations in the melt. Based on the obtained values of ε for each temperature, the experimental estimate of the viscosity (η_{exp} , Pa·s) was found; for this, a calibration curve was used, which is a graph of the dependence of η_{exp} on ε . To obtain the calibration curve, the described

experimental procedure was implemented on reference liquids with known density (2.5–3.0 g/cm³) and viscosity (0.04–12.5 Pa·s): solutions of castor oil in butyl alcohol and rosin in castor oil at $T=25$ °C, and Na₂SiO₃ and CaSiO₃ melts at $T=1300$ – 1600 °C [13,28,62]. When organic liquids were used, a thermostat with a water bath was used instead of a furnace to maintain the desired temperature in the crucible.

According to the results of the experiment, an array of pairs of values $T_i-\eta_{\text{exp},i}^l$ was obtained, where i is a serial number of measurements by temperature ($i=1-N$), and l is the number of measurements at each temperature ($l=1-3$). The arithmetic mean ($\eta_{\text{exp},i}$, Pa·s) of $\eta_{\text{exp},i}^l$ values obtained for the i -th temperature in the three series of measurements was taken as the final estimate of the viscosity for this temperature (confidence limits for its deviation from the average were calculated at the significance level $\alpha=5\%$). After the end of the experiment, the spindle (8) was removed from the melt using the lifter (27), and the crucible was cooled and its contents were ground according to the method used for slag preparation. The resulting powder (particles <0.1 mm in size) sample was sent to study the chemical composition.

To obtain original empirical models describing the temperature changes of the viscosity of the primary model slags in the considered temperature range, the experimental data were processed using Weimann–Frenkel–Urbain equation [18,25,64]:

$$\eta = AT \exp\left(\frac{E_\eta}{RT}\right) \quad (11)$$

where E_η (J/mol) is the activation energy of the viscous flow, A (Pa·s·K⁻¹) is the pre-exponential factor, R (J·mol⁻¹·K⁻¹) is the molar gas constant, and T (K) is the thermodynamic temperature. For this purpose, for each of the primary slags, the temperature-independent parameters $\ln A_{\text{OM}}$ and $E_{\eta,\text{OM}}/R$ of the paired linear regression were estimated for the theoretical model constructed from pairs of observed values $\ln(\eta_{\text{exp},i}/T_i)-1/T_i$:

$$\ln \frac{\eta_{\text{exp},i}}{T_i} = \ln A_{\text{OM}} + \frac{E_{\eta,\text{OM}}}{R} \frac{1}{T_i} \quad (12)$$

The parameters and their confidence limits (at the significance level $\alpha=5\%$) were evaluated by the least squares method, the quality of the assessment was monitored by the determination coefficient (R^2)

value, and the statistical significance (at $\alpha=5\%$) of the regression parameters and the model as a whole was determined by the P -value (P) and Fisher–Snedecor statistics (F). The values of A_{OM} and $E_{\eta,\text{OM}}$ were substituted into the equation (12); as a result, the original empirical model was derived:

$$\eta_{\text{OM}} = A_{\text{OM}} T \exp\left(\frac{E_{\eta,\text{OM}}}{RT}\right) \quad (13)$$

where η_{OM} (Pa·s) is the value of the viscosity determined by the model.

To verify the calculation models, the values of the viscosity predicted by each of them ($\eta_{\text{calc},i}$) at the corresponding temperature (T_i) were found, pairs of numbers $\eta_{\text{calc},i}-\eta_{\text{exp},i}$ were plotted on the coordinate plane, and the value of the average relative error (ε , %) was calculated according to the formula:

$$\varepsilon = 100 \frac{1}{N} \sum_{i=1}^N \left| \frac{\eta_{\text{calc},i} - \eta_{\text{exp},i}}{\eta_{\text{exp},i}} \right| \quad (14)$$

3 Results and discussion

3.1 Composition and structure of slags

The results of determining the elemental composition of the initial primary model slags by the CA methods are presented in Table 3. The obtained estimates of the contents of the main components are close to those specified in the calculation of the smelting charge. Some discrepancies are associated with incompleteness of interactions between the reagents, the transition of the crucible material (Al₂O₃) into the slag, and the analysis error. The action of the latter factors leads to a slight decrease in the ASC and basicity modulus (B_{mol}) relative to those specified for iron-containing slag (2.7 instead of 2.9 for ASC and 0.7 instead of 0.9 for B_{mol}); for iron-free slag, the indicators are the same (ASC= 2.6, $B_{\text{mol}}=0.6$). At the same time, the ASC values (2.2<ASC<3.0) unambiguously show that the synthesized slags in the molten state have the structure of their ore prototypes, formed by ring silicon–oxygen anions Si₃O₉⁶⁻ and Si₄O₁₂⁸⁻ [9].

XRD patterns of cooled samples of primary model slags are shown in Fig. 2. A halo in the region of small angles indicates that each of them is based on an amorphous phase (glass). Both samples also reveal traces of crystalline phases, which include pyroxenes and silica (card numbers are

Table 3 Elemental composition of primary model slags according to CA results

Slag	Data source	Content/wt.% (mol.% in parenthesis)										ASC	B_{mol}
		SiO ₂	MgO	CaO	Al ₂ O ₃	S	Fe ₂ O ₃	FeO	Fe ⁰	Fe _{total}	MoO ₃		
Iron-containing	CA-1	47.4 (49.7)	11.8 (18.5)	8.9 (10.0)	12.5 (7.7)	–	5.0 (2.0)	13.3 (11.7)	0.4 (0.5)	14.3	–	2.7	0.7
	CA-2	48.4 (49.8)	12.0 (18.4)	7.0 (7.7)	12.2 (7.4)	0.01 (0.01)	4.7 (1.8)	16.3 (14.0)	0.4 (0.5)	16.3	1.09 (0.5)	2.7	0.7
	Scheduled	50.7 (49.3)	14.4 (20.9)	9.5 (9.9)	4.9 (2.8)	0.2 (0.4)	–	20.0 (16.3)	–	15.9	–	2.9	0.9
Iron-free	CA-1	58.3 (57.0)	16.0 (23.3)	12.5 (13.1)	9.4 (5.4)	0.7 (1.3)	–	–	–	–	–	2.6	0.6
	CA-2	65.4 (62.5)	12.5 (21.7)	9.5 (9.7)	9.4 (5.3)	0.4 (0.7)	–	–	–	0.6	0.03 (0.01)	2.4	0.5
	Scheduled	61.9 (57.2)	17.8 (24.5)	12.6 (12.5)	5.5 (3.0)	0.8 (1.4)	–	–	–	1.4 (1.4)	–	2.6	0.6

CA-1 and CA-2 are the results of CA before and after measuring the viscosity, respectively

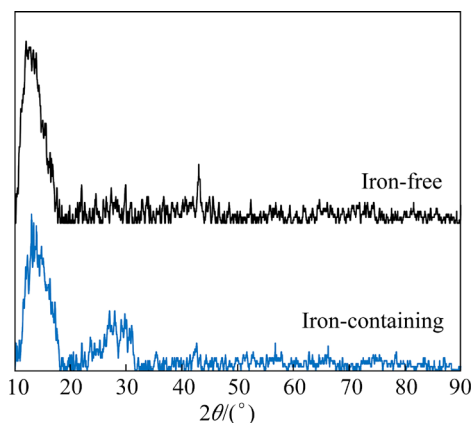


Fig. 2 XRD patterns of cooled samples of iron-containing and iron-free primary model slags

given according to Ref. [55]). These are enstatite ($\text{Ca}_{0.23}\text{Mg}_{1.77}\text{Si}_2\text{O}_6$, 00–900–5543), silica (SiO_2 , 00–412–4082) and ferrosilite (FeSiO_3 , 00–900–0481) for iron-containing slag; diopside ($\text{CaMgSi}_2\text{O}_6$, 00–101–1047) and silica (SiO_2 , 00–152–6860) for iron-free slag.

The results of studying the composition and structure of cooled primary model slags by SEM and EDS methods are shown in Figs. 3 and 4 and in Tables 4–6. The elemental composition determined by these methods is consistent with the results of CA (Table 4). The structure of the solidified iron-containing slag (Fig. 3 and Table 5) is formed by a glass matrix, the average composition of which corresponds to the empirical formula of $\text{Fe}_{0.32}\text{Ca}_{0.17}\text{Mg}_{0.35}\text{SiAl}_{0.26}\text{O}_{3.15}$. The basis of iron-free slag (Fig. 4 and Table 6) is a glass of another composition ($\text{Ca}_{0.18}\text{Mg}_{0.38}\text{SiAl}_{0.12}\text{O}_{2.73}\text{S}_{0.01}$). At the

same time, a small amount of silica and pyrrhotite crystals, released during cooling, are revealed; the volume fractions of these crystalline phases, determined by the planimetric method in sections 400 μm long and 400 μm wide, are 6.5% and 0.5%, and the average particle sizes are 1 and 0.6 μm , respectively. The recalculation of the average local elemental compositions of glasses to the compositions of minerals shows the possibility of crystallization from iron-containing slag of a mixture containing 46.6 wt.% anorthite ($\text{CaAl}_2\text{Si}_2\text{O}_8$) and 53.4 wt.% pyroxene ($\text{Fe}_{0.44}\text{Ca}_{0.06}\text{Mg}_{0.50}\text{SiO}_3$) and from iron-free slag containing 17.8 wt.% anorthite ($\text{CaAl}_2\text{Si}_2\text{O}_8$), 56.4 wt.% pyroxene ($\text{Ca}_{0.24}\text{Mg}_{0.76}\text{SiO}_3$), and 25.8 wt.% silica (SiO_2). Obviously, the removal of iron oxides from the slag

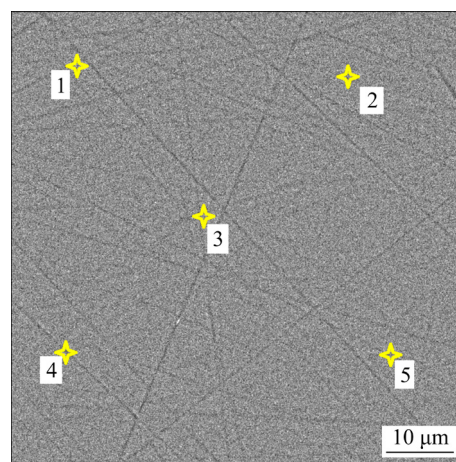


Fig. 3 SEM image of cooled sample of iron-containing primary model slag (1–5 are the points for determining local elemental composition by the EDS method)

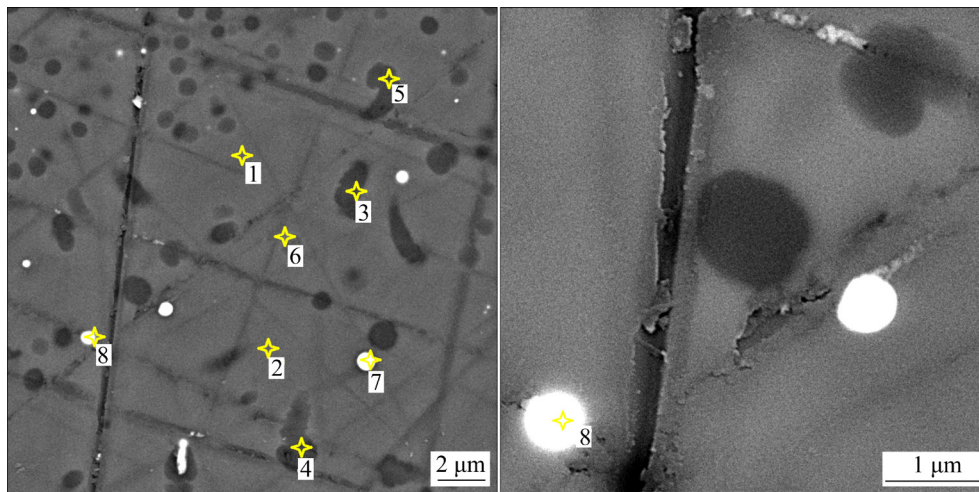


Fig. 4 SEM images of cooled sample of iron-free primary model slag (1–8 are the points for determining local elemental composition by the EDS method)

Table 4 Elemental composition of primary model slags according to EDS data (in areas of $400\ \mu\text{m} \times 400\ \mu\text{m}$)

Slag	Data source	Content/wt.%							
		Al	Ca	Fe	Mg	O	S	Si	Total
Iron-containing	EDS	6.0	5.8	14.8	7.2	42.5	–	23.7	100.0
	CA	6.6	6.4	14.3	7.1	42.8	–	22.2	99.4
	Scheduled	2.6	6.8	15.9	8.7	42.2	0.2	23.7	100.0
Iron-free	EDS	3.5	7.9	1.5	9.8	46.0	1.1	30.2	100.0
	CA	5.0	8.9	n. d.	9.7	45.4	0.7	27.2	96.9
	Scheduled	2.9	9.0	1.4	10.7	46.2	0.8	28.9	100.0

Table 5 Local elemental composition of iron-containing primary model slag and empirical formulas of identified phases for Points 1–5 according to Fig. 3

Point	Content/wt.%						Phase
	O	Mg	Al	Si	Ca	Fe	
1	42.8	7.2	5.8	23.8	5.9	14.6	$\text{Fe}_{0.31}\text{Ca}_{0.17}\text{Mg}_{0.35}\text{SiAl}_{0.26}\text{O}_{3.16}$
2	42.0	7.4	5.9	23.6	5.9	15.3	$\text{Fe}_{0.32}\text{Ca}_{0.17}\text{Mg}_{0.36}\text{SiAl}_{0.26}\text{O}_{3.12}$
3	43.2	7.4	6.1	23.2	5.9	14.2	$\text{Fe}_{0.31}\text{Ca}_{0.18}\text{Mg}_{0.37}\text{SiAl}_{0.27}\text{O}_{3.27}$
4	42.8	7.4	6.0	23.9	5.7	14.3	$\text{Fe}_{0.30}\text{Ca}_{0.17}\text{Mg}_{0.36}\text{SiAl}_{0.26}\text{O}_{3.14}$
5	42.5	7.5	6.3	23.8	5.5	14.5	$\text{Fe}_{0.31}\text{Ca}_{0.16}\text{Mg}_{0.36}\text{SiAl}_{0.27}\text{O}_{3.13}$

Table 6 Local elemental composition of iron-free primary model slag and empirical formulas of identified phases for Points 1–8 according to Fig. 4

Point	Content/wt.%							Phase
	O	Mg	Al	Si	S	Ca	Fe	
1	47.6	9.7	3.4	32.0	–	7.4	–	$\text{Ca}_{0.16}\text{Mg}_{0.35}\text{SiAl}_{0.11}\text{O}_{2.61}$
2	47.8	10.7	3.6	29.0	0.6	8.2	–	$\text{Ca}_{0.20}\text{Mg}_{0.43}\text{SiAl}_{0.13}\text{O}_{2.89}\text{S}_{0.02}$
3	50.6	5.2	2.0	38.4	–	3.8	–	SiO_2
4	50.2	5.9	2.1	36.8	–	5.0	–	SiO_2
5	49.9	7.1	2.6	34.3	0.6	5.6	–	SiO_2
6	48.1	9.5	3.4	31.1	0.6	7.4	–	$\text{Ca}_{0.17}\text{Mg}_{0.35}\text{SiAl}_{0.11}\text{O}_{2.71}\text{S}_{0.02}$
7	–	–	–	–	44.2	–	55.8	F_{1-x}S
8	–	–	–	–	42.7	–	57.3	F_{1-x}S

shifts the pyroxene composition toward diopside ((Ca,Mg)SiO₃), increases the amount of anorthite, and releases part of the silica.

In general, the results of studying the material composition of cooled primary model slags, carried out by the XRD, SEM, and EDS methods, confirm the conclusion made on the basis of the assessment of the ASC value about the nature of their structure in a molten state.

The elemental composition (in mole fractions) of primary model slags and transitional slags formed by removing 20%–80% of iron oxides from iron-containing primary slag (by calculation) is presented in Table 7 and Fig. 5. From these data, the exclusion of up to 80% of iron-containing phases from the slag composition (from 0.02 to 0.00 for Fe₂O₃, and from 0.12 to 0.02 for FeO) is accompanied by a uniform (almost linear) increase in mole fractions of the remaining components (from 0.51 to 0.56 for SiO₂, from 0.19 to 0.21 for MgO, from 0.10 to 0.11 for CaO, and from 0.08 to 0.09 for Al₂O₃). In this case, the ASC and B_{mol} decrease from 2.7 to 2.5 and from 0.7 to 0.5, respectively. In the transition from slag with IRC of 80% to iron-free primary slag (IRC=100%, ASC=2.6, B_{mol} =0.6), an intensification of the growth of MgO, CaO and a decrease of Al₂O₃ is noted, the mole fractions of which eventually take on the values of 0.24, 0.13, and 0.05, respectively

Table 7 Elemental composition (in mole fractions) of primary and transitional model slags, normalized on amounts of oxides

Component	X					
	IRC=0%	IRC=20%	IRC=40%	IRC=60%	IRC=80%	IRC=100%
SiO ₂	0.50	0.51	0.53	0.54	0.56	0.58
MgO	0.19	0.19	0.20	0.20	0.21	0.24
CaO	0.10	0.10	0.11	0.11	0.11	0.13
Al ₂ O ₃	0.08	0.08	0.08	0.08	0.09	0.05
Fe ₂ O ₃	0.02	0.02	0.01	0.01	0.00	0.00
FeO	0.12	0.10	0.07	0.05	0.02	0.00
ASC	2.7	2.7	2.6	2.6	2.5	2.6
B_{mol}	0.7	0.7	0.6	0.6	0.5	0.6

The initial compositions of primary model slags were recalculated from the CA results

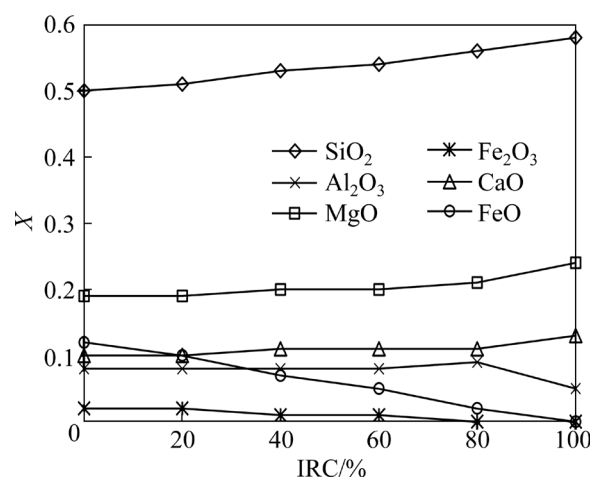


Fig. 5 Curves of changes in elemental composition of iron-containing model slag depending on iron oxides removal completeness

(the portion of SiO₂ is at the level of 0.56–0.58); this fact is probably related to the fluctuations in the composition taking place during the preparation of the prototype and the error in weighing the components of the ore smelting charge, as well as the possible reduction of a part of SiO₂. In general, variation in the composition of slags does not cause the ASC value to go beyond the range of 2.2–3.0, which indicates the absence of the significant differences in their structure [9].

3.2 Thermal properties of slags

DSC heating curves (30–1450 °C, $\beta=20$ °C/min) of primary model slags in the temperature range of 1000–1450 °C are shown in Fig. 6. The complex endothermic peaks revealed on them correspond to the melting of crystalline phases precipitated during cold crystallization (the identification of compounds was out of the scope of this work) and have the following characteristics: $T_o=1119$ °C, $T_{p,1}=1181$ °C, and $T_e=1260$ °C for iron-containing slag, $T_o=1148$ °C, $T_{p,1}=1241$ °C, $T_{p,2}=1313$ °C, and $T_e=1360$ °C for iron-free slag. Peak separation (Figs. 7 and 8) makes it possible to establish refined temperatures of the maxima of their constituent elementary peaks: $T_{p,1}^r=(1168\pm4)$ °C, $T_{p,2}^r=(1183\pm1)$ °C, and $T_{p,3}^r=(1213\pm2)$ °C for iron-containing slag, $T_{p,1}^r=(1227\pm1)$ °C and $T_{p,2}^r=(1315\pm1)$ °C for iron-free slag. The liquidus temperatures of these slags determined from these data are (1213±2) and (1315±1) °C, respectively. Therefore, it can be assumed that, above the temperatures of 1300 and

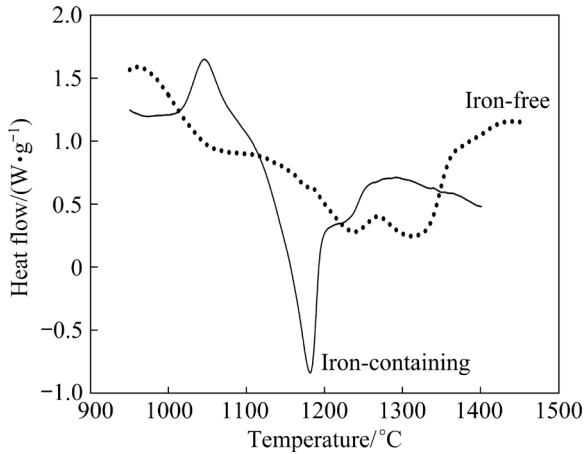


Fig. 6 DSC curves of heating (950–1450 °C, $\beta=20$ °C/min, argon) of iron-containing and iron-free primary model slags

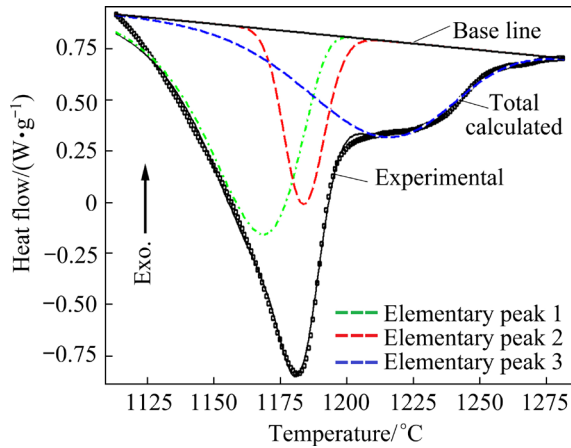


Fig. 7 Separation results ($r=0.9984$) for complex endothermic peak (1113–1282 °C) on DSC curve of heating (950–1450 °C, $\beta=20$ °C/min, argon) of iron-containing primary model slag

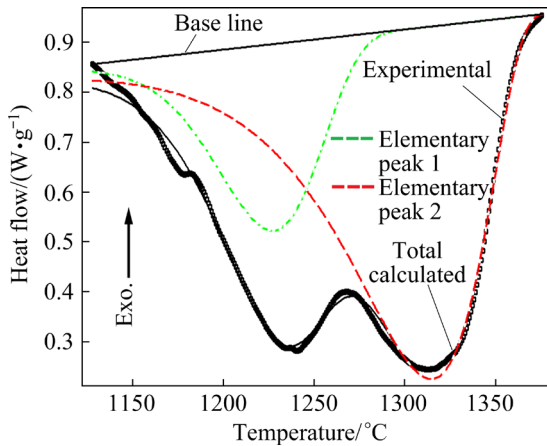


Fig. 8 Separation results ($r=0.9976$) for complex endothermic peak (1128–1376 °C) on DSC curve of heating (950–1450 °C, $\beta=20$ °C/min, argon) of iron-free primary model slag

1400 °C, respectively, the melts of iron-containing and iron-free primary samples are guaranteed to be homogeneous and have the properties of a Newtonian fluid [34]. In this regard, the theoretical and experimental determination of their viscosity was carried out at temperatures exceeding the indicated marks (for the iron-free sample, additional calculations were performed in the range of 1300–1400 °C).

3.3 Theoretical viscosity values of slags

Based on the data from Table 7, the Kalmanovitch–Frank model for iron-containing primary model slag can be represented by the equation:

$$\eta_{\text{KFM}} = 6.27 \times 10^{-10} T \exp\left(\frac{25107}{T}\right) \quad (15)$$

And for the iron-free sample, it takes the following form:

$$\eta_{\text{KFM}} = 5.22 \times 10^{-10} T \exp\left(\frac{25759}{T}\right) \quad (16)$$

The calculation results using this model (Table 8 and Fig. 9) show that with decrease in temperature from 1550 to 1300 °C, the predicted values of the viscosity of iron-containing slag increase within the range of 1.09–8.43 Pa·s. A comparison of these data with the results of the experimental assessment (continuous cooling, vibrational method) of the viscosity of artificial slags of similar basicity (53.4–54.8 wt.% SiO₂, 22.7–25.2 wt.% CaO, 2.7–2.8 wt.% MgO, 12.7–17.1 wt.% FeO, and 4.0–4.6 wt.% Al₂O₃, $B_{\text{mol}}=0.7$ –0.8), simulating slags from the smelting of oxidized cobalt–nickel ores [42], shows satisfactory agreement only for 1500 °C: $\eta_{\text{exp}}=1.2$ –1.6 Pa·s [42] and $\eta_{\text{KFM}}=1.57$ Pa·s in this work; as the temperature drops to 1300 °C, discrepancy increases significantly: $\eta_{\text{exp}}=2.0$ –2.3 Pa·s [42] and $\eta_{\text{KFM}}=8.43$ Pa·s in this work. For iron-free slag, the values of η_{KFM} at 1550–1400 °C are somewhat higher and amount to 1.30–4.24 Pa·s. This satisfactorily agrees with the data on the viscosity of slags of similar compositions and basicity (60 wt.% SiO₂, 10–15 wt.% CaO, 15–20 wt.% MgO, and 10 wt.% Al₂O₃, $B_{\text{mol}}=0.6$) obtained by the rotational method by MACHIN and YEE [12]: at 1500 °C, $\eta_{\text{exp}}=2.48$ –2.85 Pa·s [12] and $\eta_{\text{KFM}}=1.89$ Pa·s in this work; at 1450 °C, $\eta_{\text{exp}}=3.83$ –4.27 Pa·s [12] and $\eta_{\text{KFM}}=2.80$ Pa·s in this work.

The assessment of compositional changes in the viscosity of the studied slags within the framework of the Kalmanovitch–Frank model shows (Table 9 and Fig. 10) that in the temperature range of 1400–1550 °C, a continuous transition from iron-containing primary slag to slag with IRC=80% is possible while maintaining the viscosity level (up to 70 dPa·s), which provides favorable conditions for the separation of products of industrial electric smelting of copper–nickel raw materials [65]. For temperatures of 1550, 1500, 1450, and 1400 °C, the predicted values of η_{KFM} during such a transition increase in the ranges of 1.09–2.02, 1.57–3.00, 2.30–4.56, and 3.45–7.13 Pa·s, respectively. Deeper removal of iron oxides can lead to a sharp increase in viscosity, which requires the addition of calcium or magnesium oxides; for example, until the

composition of the iron-free primary model slag is reached, the calculated η_{KFM} value of which at 1400 °C is 42.4 dPa·s. The resulting pattern correlates with the effect of iron oxides removal completeness on the calculated viscous flow temperature coefficient (B_{KFM}) (Fig. 11). Thus, with an increase in the IRC value from 0 to 80%, the B_{KFM} value increases from 25.107 to 27.397 K, which is associated with enlargement of silicon–oxygen complexes against the background of a growing deficiency of modifier cations [9,18,34]. It should be emphasized that the data obtained confirm the fact of changes in the viscosity of slags in the absence of significant structural rearrangement [19,34]. It is also obvious that the Kalmanovitch–Frank model is insensitive to the mutual replacement of modifier cations (Fe^{2+} , Mg^{2+} , and Ca^{2+}).

Table 8 Experimental and calculated viscosity of primary model slags at 1300–1550 °C (Pa·s)

No.	Temperature/°C	Iron-containing slag			Iron-free slag		
		η_{exp}	η_{OM}	η_{KFM}	η_{exp}	η_{OM}	η_{KFM}
1	1550	0.31 ± 0.23	0.34	1.09	1.28 ± 0.05	1.17	1.30
2	1525	0.39 ± 0.12	0.41	1.31	1.36 ± 0.07	1.43	1.56
3	1500	0.46 ± 0.09	0.49	1.57	1.67 ± 0.37	1.77	1.89
4	1475	0.62 ± 0.06	0.59	1.89	2.19 ± 0.19	2.19	2.29
5	1450	0.73 ± 0.13	0.71	2.30	2.65 ± 0.59	2.73	2.80
6	1425	1.02 ± 0.40	0.87	2.81	3.43 ± 0.31	3.43	3.43
7	1400	1.24 ± 0.16	1.06	3.45	4.55 ± 0.34	4.34	4.24
8	1375	1.35 ± 0.28	1.31	4.27	–	–	–
9	1350	1.57 ± 0.56	1.62	5.32	–	–	–
10	1325	1.86 ± 0.68	2.02	6.67	–	–	–
11	1300	2.33 ± 0.37	2.54	8.43	–	–	–

Confidence limits for η_{exp} are given for $\alpha=5\%$

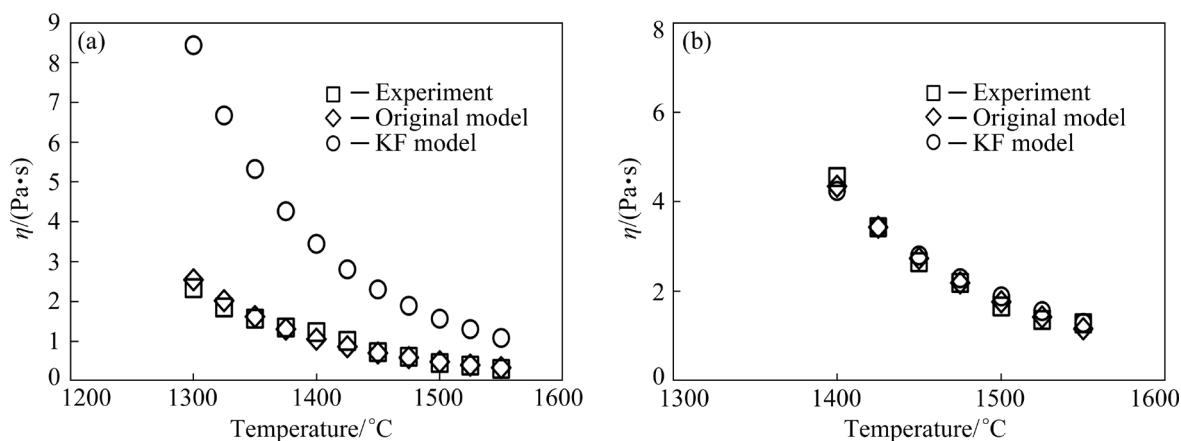
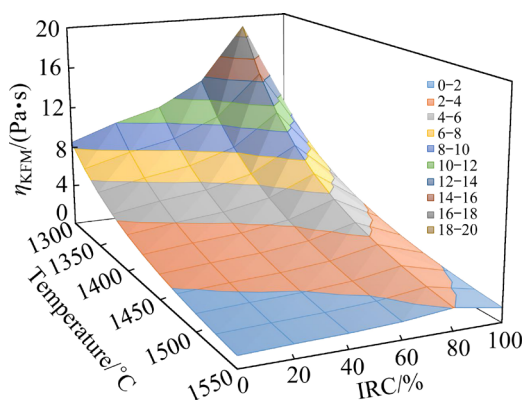
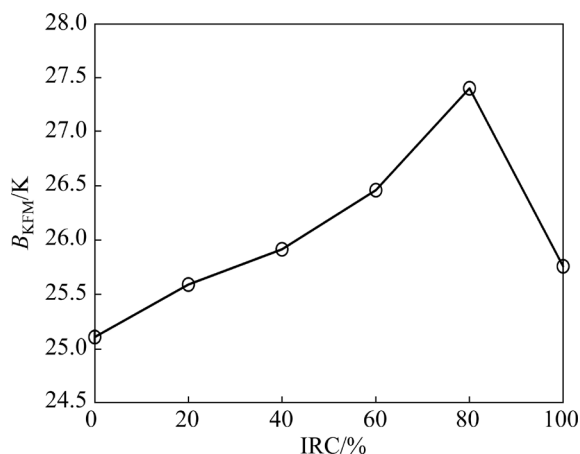


Fig. 9 Experimental and calculated curves of temperature changes of viscosity of iron-containing (a) and iron-free (b) primary model slags

Table 9 Results of viscosity prediction (Kalmanovitch–Frank model) of primary and transition model slags at 1300–1550 °C

No.	Temperature/°C	$\eta_{\text{KFM}}/(\text{Pa}\cdot\text{s})$					
		IRC=0%	IRC=20%	IRC=40%	IRC=60%	IRC=80%	IRC=100%
1	1550	1.09	1.25	1.36	1.57	2.02	1.30
2	1525	1.31	1.49	1.63	1.89	2.45	1.56
3	1500	1.57	1.80	1.97	2.30	3.00	1.89
4	1475	1.89	2.18	2.40	2.81	3.69	2.29
5	1450	2.30	2.66	2.93	3.45	4.56	2.80
6	1425	2.81	3.26	3.60	4.26	5.68	3.43
7	1400	3.45	4.02	4.46	5.29	7.13	4.24
8	1375	4.27	5.00	5.56	6.63	9.00	5.28
9	1350	5.32	6.25	6.97	8.36	11.45	6.62
10	1325	6.67	7.88	8.81	10.62	14.68	8.36
11	1300	8.43	10.00	11.22	13.60	18.98	10.62
$\ln[A_{\text{KFM}}/(\text{Pa}\cdot\text{s}\cdot\text{K}^{-1})]$		-21.19	-21.33	-21.42	-21.57	-21.83	-21.37
B_{KFM}/K		25.107	25.591	25.915	26.458	27.397	25.759

**Fig. 10** Calculated (Kalmanovitch–Frank model) surface of change of viscosity of model slags depending on temperature and iron oxides removal completeness**Fig. 11** Dependence curve of calculated (Kalmanovitch–Frank model) temperature coefficient of viscosity of model slags on iron oxides removal completeness

3.4 Experimental viscosity values of slags

The results of the experimental viscosity assessment of primary model slags are presented in Table 8 and Fig. 9 (it should be noted that, as shown in Table 3, no significant changes in the chemical composition of the slags are detected during the experiment; a slight transition of the crucible material into the melt is noted (at the level of 0.03–1.09 wt.% MoO_3); differences in the contents of the remaining components are associated with the determination error; the values of the ASC (ASC=2.7 for iron-containing slag and ASC=2.4 for iron-free slag) and basicity modulus ($B_{\text{mol}}=0.7$ for iron-containing slag and $B_{\text{mol}}=0.5$ for iron-free slag) are close to the initial values). It follows from these data that with a decrease in the temperature from 1550 to 1300 °C, the viscosity of the iron-containing sample naturally increases from 0.31 to 2.33 Pa·s. For the iron-free sample, the temperature dependence of viscosity is similar, but the absolute values of η are much higher ($\eta_{\text{exp}}=1.28$ Pa·s at 1550 °C and $\eta_{\text{exp}}=4.55$ Pa·s at 1400 °C), which corresponds to the results of Ref. [12] for oxide systems similar in composition, given in the analysis of the results of theoretical modeling. In both cases, the viscosity of the melts is at a level that ensures the efficient operation of electric furnaces for matte smelting [65]. Based on the experimental data, the Arrhenius plots (Fig. 12) are constructed and the values of the pre-exponential

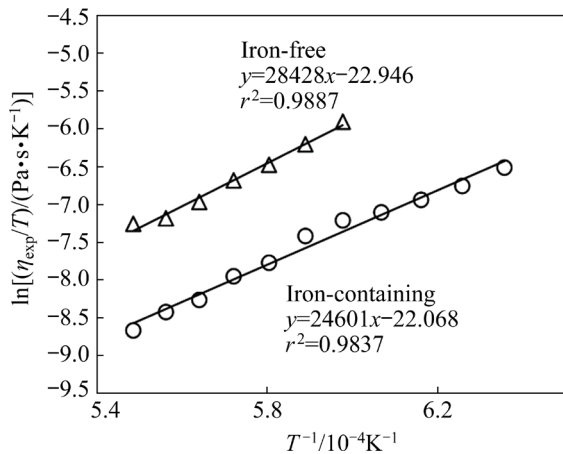


Fig. 12 Arrhenius plots constructed from experimental values of viscosity of iron-containing and iron-free primary model slags

factor and activation energy of the viscous flow are determined: $\ln A_{OM}=(-22.1\pm 1.4) \text{ Pa}\cdot\text{s}\cdot\text{K}^{-1}$ and $E_{\eta,OM}=(204\pm 20) \text{ kJ/mol}$ for iron-containing slag, $\ln A_{OM}=(-22.9\pm 2.0) \text{ Pa}\cdot\text{s}\cdot\text{K}^{-1}$ and $E_{\eta,OM}=(236\pm 29) \text{ kJ/mol}$ for iron-free slag. From these data, the value of the activation energy for the iron-free sample is naturally higher, which is associated with its lower basicity ($B_{\text{mol}}=0.6$); this fact is in agreement with the known data on the increase in E_{η} with a decrease in basicity associated with rising of slag structure polymerization [17,34]. The values of $E_{\eta,OM}$ are in the range of 154–270 kJ/mol, which is typical for melts of the CaO–MgO–Al₂O₃–SiO₂ and CaO–MgO–FeO_x–Al₂O₃–SiO₂ systems [17,27]. As a result, original empirical models are obtained that describe temperature changes in the viscosity of primary model slags for iron-containing slag:

$$\eta_{OM}=2.61\times 10^{-10} T \exp\left(\frac{24601}{T}\right) \quad (17)$$

And for iron-free slag:

$$\eta_{OM}=1.08\times 10^{-10} T \exp\left(\frac{28428}{T}\right) \quad (18)$$

The value of the coefficient of determination ($r^2=0.9837$ – 0.9887) indicates a high reliability of estimates. P -values for the intercept ($P_0=5.7\times 10^{-11}$ for Eq. (17) and $P_0=8.4\times 10^{-7}$ for Eq. (18)) and the coefficient for the explanatory regression variable ($P_1=2.3\times 10^{-9}$ for Eq. (17) and $P_1=4.6\times 10^{-6}$ for Eq. (18)) are below the accepted significance level ($\alpha=0.05$), and the Fisher–Snedecor statistics ($F=542.9$ for Eq. (17) and $F=437.5$ for Eq. (18))

exceeds the critical value ($F_{\text{crit}}=5.1$ for Eq. (17) and $F_{\text{crit}}=230.2$ for Eq. (18)); based on this, conclusion on the statistical significance of the regression parameters and regression equations as a whole at the significance level $\alpha=5\%$ can be done. Estimates of the viscosity (η_{OM}) for iron-containing slag within the obtained model show an increase from 0.34 Pa·s at 1550 °C to 2.54 Pa·s at 1300 °C; for iron-free slag, the corresponding values vary from 1.17 Pa·s at 1550 °C to 4.34 Pa·s at 1400 °C (Table 8 and Fig. 9).

3.5 Models verification

Verification of the models used in relation to the problem of predicting the viscosity of primary model slags in the temperature range of 1300–1550 °C shows high reliability ($\varepsilon=7\%$ for iron-containing slag and $\varepsilon=4\%$ for iron-free slag) of the original models (Fig. 13). A significant average error of the Kalmanovitch–Frank model for iron-containing slag ($\varepsilon=225\%$) is associated with an overestimation of viscosity in the considered range

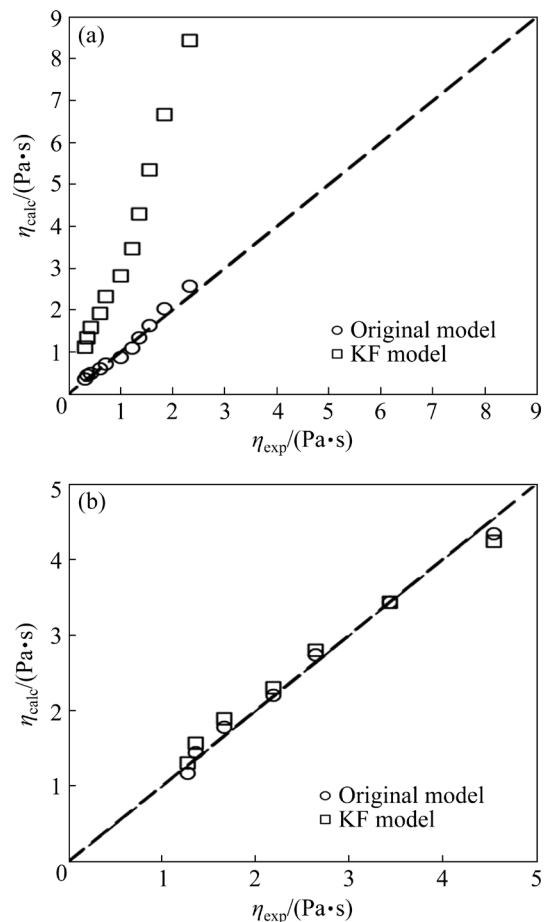


Fig. 13 Comparison of calculated and experimental viscosity of iron-containing (a) and iron-free (b) primary model slags

of compositions, which most likely occurs due to the insufficient consideration of the action of a number of factors. At the same time, for iron-free slag ($\varepsilon=7\%$), the forecast turns out to be quite accurate. It should be noted that the sulfur contained in the iron-free primary model slag does not seem to have any effect on its viscous characteristics, while its effect cannot be ruled out in relation to the iron-containing sample. The model verification results allow one to conclude that the calculated estimates within the framework of the Kalmanovitch–Frank model can be taken as upper boundary estimates of the true viscosity of model slags in the considered range of temperatures and compositions. And based on the fact that the latter has the structure of real prototypes, the revealed patterns of temperature-compositional changes in their properties can be extended to real slags. In this regard, it can be concluded that in order to obtain slags with optimal technological characteristics, joint contractile smelting of oxidized nickel and sulfide copper ores of the studied compositions should be carried out at temperatures of about 1400 °C.

4 Conclusions

(1) Iron-containing and iron-free primary model slags have been synthesized, which are close to real slags of the joint smelting of oxidized nickel and sulfide copper ores in terms of the content of the main components. The values of the ASC ($ASC=2.6-2.9$) and the basicity modulus ($B_{mol}=0.6-0.8$) of model samples and real prototypes indicate the unity of the structure of their melts, determined by the presence of ring silicon–oxygen anions $Si_3O_9^{6-}$ and $Si_4O_{12}^{8-}$. It is confirmed that, above 1300 and 1400 °C, respectively, the melts of iron-containing and iron-free primary model slags have the properties of a Newtonian fluid.

(2) Prediction by the Kalmanovitch–Frank model shows that the predicted values of the viscosity of iron-containing (1550–1300 °C) and iron-free (1550–1400 °C) primary model slags are in the range of 1.09–8.43 and 1.30–4.24 Pa·s, respectively. In the range of 1400–1550 °C, a continuous transition from iron-containing primary model slag to slag with IRC=80% is possible while maintaining the viscosity level no higher than

7.0 Pa·s. With a deeper removal of iron oxides, it is necessary to adjust the composition by adding calcium or magnesium oxides.

(3) Experimental viscosity estimates of iron-containing (1550–1300 °C) and iron-free (1550–1400 °C) primary model slags are in the ranges of 0.31–2.33 and 1.28–4.55 Pa·s, respectively. Reducing the basicity from $B_{mol}=0.7$ (iron-containing slag) to $B_{mol}=0.6$ (iron-free slag) increases the activation energy of the viscous flow from 204 to 236 kJ/mol.

(4) In the considered range of temperatures and compositions, the Kalmanovitch–Frank model gives upper boundary estimates ($\varepsilon=7\%-225\%$) of the viscosity of model and real slags. Original empirical models make it possible to obtain refined ($\varepsilon=4\%-7\%$) viscosity values for primary model slags.

(5) To obtain slags of optimal viscosity, joint contractile smelting of oxidized nickel and sulfide copper ores of the studied compositions should be carried out at a temperature not lower than 1400 °C.

(6) The results obtained can be used in the development and improvement of pyrometallurgical processing technologies of mineral and technogenic raw materials of non-ferrous and ferrous metallurgy, as well as in the glass-making and ceramics industries.

Acknowledgments

This work was carried out according to the State Assignment for IMET UB RAS (Theme State Registration No. 122020100404-2) using the equipment of the Collaborative Usage Center “Ural–M”.

References

- [1] DUNN J G, JAYAWEERA S A A. Effect of heating rate on the TG curve during the oxidation of nickel sulphide concentrates [J]. *Thermochimica Acta*, 1983, 61: 313–317.
- [2] SELIVANOV E N, KLYUSHNIKOV A M, GULYAEVA R I. Application of sulfide copper ores oxidizing roasting products as sulfidizing agent during melting nickel raw materials to matte [J]. *Metallurgist*, 2019, 63(7/8): 867–877.
- [3] EVERAERT M, LEMMENS V, ATIA T A, SPOOREN J. Sulfidic mine tailings and marl waste rock as compatible resources in a microwave-assisted roasting process [J]. *Journal of Cleaner Production*, 2020, 274: 122628.
- [4] IZYDORCZYK G, MIKULA K, SKRZYPCZAK D, MOUSTAKAS K, WITEK-KROWIAK A, CHOJNACKA K. Potential environmental pollution from copper metallurgy

- and methods of management [J]. *Environmental Research*, 2021, 197: 111050.
- [5] KLYUSHNIKOV A M, GULYAEVA R I, SELIVANOV E N, PIKALOV S M. Kinetics and mechanism of oxidation for nickel-containing pyrrhotite tailings [J]. *International Journal of Minerals, Metallurgy and Materials*, 2021, 28(9): 1469–1477.
- [6] KLYUSHNIKOV A M. Modeling of exchange interactions in melts formed during joint smelting of oxidized nickel ores and pyrrhotite concentrates [J]. *Metallurgist*, 2022, 66(1/2): 190–199.
- [7] KLYUSHNIKOV A M, GULYAEVA R I, PIKALOV S M. Cold crystallization kinetics of slag from the joint smelting of oxidized nickel and sulfide copper ores [J]. *Journal of Thermal Analysis and Calorimetry*, 2022. 147: 12165–12176.
- [8] SELIVANOV E N, GULYAEVA R I, KLYUSHNIKOV A M. Study of structure and phase composition of copper–cobalt sulfide ores of Dergamyshskoe deposit [J]. *Tsvetnye Metally*, 2016, 2016(3): 13–17.
- [9] REZNIK I D, SOBOL S I, KHUDYAKOV V M. Cobalt: in two volumes: Volume 1 [M]. Moscow: Mashinostroenie, 1995 (in Russian).
- [10] MACHIN J S, HANNA D L. Viscosity studies of the system CaO–MgO–Al₂O₃–SiO₂. I: 40% SiO₂ [J]. *Journal of the American Ceramic Society*, 1945, 29: 1–14.
- [11] MACHIN J S, YEE T B, HANNA D L. Viscosity studies of system CaO–MgO–Al₂O₃–SiO₂. III: 35, 45, and 50% SiO₂ [J]. *Journal of the American Ceramic Society*, 1953, 31: 200–204.
- [12] MACHIN J S, YEE T B. Viscosity studies of system CaO–MgO–Al₂O₃–SiO₂. IV: 60 and 65% SiO₂ [J]. *Journal of the American Ceramic Society*, 1954, 37: 177–186.
- [13] ARMAN, TSURUDA A, ARMA L H, TAKEBE H. Viscosity measurement and prediction of gasified and synthesized coal slag melts [J]. *Fuel*, 2017, 200: 521–528.
- [14] CHEN Mao, RAGHUNATH S, ZHAO Bao-jun. Viscosity measurements of “FeO”–SiO₂ slag in equilibrium with metallic Fe [J]. *Metallurgical and Materials Transactions B*, 2013, 44: 506–515.
- [15] CHEN Zi-wei, WANG Hao, SUN Yong-qi, LIU Li, WANG Xi-dong. Insight into the relationship between viscosity and structure of CaO–SiO₂–MgO–Al₂O₃ molten slags [J]. *Metallurgical and Materials Transactions B*, 2019, 50: 2930–2941.
- [16] CHEN Yong-feng, LV Xue-ming, PANG Zheng-de, LV Xue-wei. Effect of basicity and Al₂O₃ on viscosity of ferronickel smelting slag [J]. *Journal of Iron and Steel Research International*, 2020, 27: 1400–1406.
- [17] GAO Yun-ming, WANG Shao-bo, HONG Chuan, MA Xiu-juan, YANG Fu. Effects of basicity and MgO content on the viscosity of the SiO₂–CaO–MgO–9wt.%Al₂O₃ slag system [J]. *International Journal of Minerals, Metallurgy and Materials*, 2014, 21(4): 353–362.
- [18] HAN Chen, CHEN Mao, ZHANG Wei-dong, ZHAO Zhi-xing, EVANS T, ZHAO Bao-jun. Evaluation of existing viscosity data and models and developments of new viscosity model for fully liquid slag in the SiO₂–Al₂O₃–CaO–MgO system [J]. *Metallurgical and Materials Transactions B*, 2016, 47: 2861–2874.
- [19] HOCELLA M F, BROWN G E. Structure and viscosity of rhyolitic composition melts [J]. *Geochimica et Cosmochimica Acta*, 1984, 48: 2631–2640.
- [20] JI F Z, SICHEN Du, SEETHARAMAN S. Experimental studies of the viscosities in the CaO–Fe_nO–SiO₂ slags [J]. *Metallurgical and Materials Transactions B*, 1997, 28: 827–834.
- [21] JI F Z, SICHEN Du, SEETHARAMAN S. Viscosities of multicomponent silicate melts at high temperatures [J]. *International Journal of Thermophysics*, 1999, 20: 309–323.
- [22] KIM H, MATSUURA H, TSUKIHASHI F, WANG W, MIN D J, SOH I. Effect of Al₂O₃ and CaO/SiO₂ on the viscosity of calcium-silicate-based slags containing 10 mass pct MgO [J]. *Metallurgical and Materials Transactions B*, 2013, 44: 5–12.
- [23] KO H, KIM M, PARK S M, LIM H M. High-temperature viscosity analysis of aluminosilicate melts and the comparison to empirical models [J]. *Journal of the Korean Ceramic Society*, 2020, 58: 160–168.
- [24] KONDRATIEV A, JAK E. Review of experimental data and modeling of the viscosities of fully liquid slags in the Al₂O₃–CaO–‘FeO’–SiO₂ system [J]. *Metallurgical and Materials Transactions B*, 2001, 32: 1015–1025.
- [25] KONDRATIEV A, KHVAN A V. Analysis of viscosity equations relevant to silicate melts and glasses [J]. *Journal of Non-Crystalline Solids*, 2016, 432: 366–383.
- [26] KONG Ling-xue, BAI Jin, LI Wen. Viscosity-temperature property of coal ash slag at the condition of entrained flow gasification: A review [J]. *Fuel Processing Technology*, 2021, 215: 106751.
- [27] KOWALCZYK J, MROZ W, WARCZOK A, UTIGARD T A. Viscosity of copper slags from chalcocite concentrate smelting [J]. *Metallurgical and Materials Transactions B*, 1995, 26: 1217–1223.
- [28] MIZOGUCHI K, YAMANE M, SUGINOHARA Y. Viscosity measurements of the molten MeO(Me=Ca, Mg, Na)–SiO₂–Ga₂O₃ silicate system [J]. *Journal of the Japan Institute of Metals*, 1986, 50(1): 76–82.
- [29] PARK J H, MIN D J, SONG H S. Amphoteric behavior of alumina in viscous flow and structure of CaO–SiO₂(–MgO)–Al₂O₃ slags [J]. *Metallurgical and Materials Transactions B*, 2004, 35: 269–275.
- [30] PARK H S, PARK S S, SOHN I. The viscous behavior of FeO–Al₂O₃–SiO₂ copper smelting slags [J]. *Metallurgical and Materials Transactions B*, 2011, 42: 692–699.
- [31] PENGCHENG Li, XIAOJUN Ning. Effects of MgO/Al₂O₃ ratio and basicity on the viscosities of CaO–MgO–SiO₂–Al₂O₃ slags: Experiments and modeling [J]. *Metallurgical and Materials Transactions B*, 2016, 47: 446–657.
- [32] SELIVANOV E, GULYAEVA R, ISTOMIN S, BELYAEV V, TYUSHNYAKOV S, BYKOV A. Viscosity and thermal properties of slag in the process of autogenous smelting of copper–zinc concentrates [J]. *Mineral Processing and Extractive Metallurgy*, 2015, 125(2): 88–95.
- [33] TANG Xu-long, ZHANG Zuo-tai, GUO Min, ZHANG Mei, WANG Xi-dong. Viscosities behavior of CaO–SiO₂–MgO–Al₂O₃ slag with low mass ratio of CaO to SiO₂ and wide range of Al₂O₃ content [J]. *Journal of Iron and Steel Research International*, 2011, 18: 1–6.

- [34] VARGAS S, FRANSEN F J, DAM-JOHANSEN K. Rheological properties of high-temperature melts of coal ashes and other silicates [J]. *Progress in Energy and Combustion Science*, 2001, 27: 237–429.
- [35] VIDACAK B, DU Si-chen, SEETHARAMAN S. An experimental study of the viscosities of $\text{Al}_2\text{O}_3\text{-CaO-“FeO”}$ slags [J]. *Metallurgical and Materials Transactions B*, 2001, 32: 679–684.
- [36] WANG Zhaan-jun, SUN Yong-qi, SRIDHAR S, ZHANG Mei, GUO Min, ZHANG Zuo-tai. Effect of Al_2O_3 on the viscosity and structure of $\text{CaO-SiO}_2\text{-MgO-Al}_2\text{O}_3\text{-Fe}_2\text{O}_3$ slags [J]. *Metallurgical and Materials Transactions B*, 2015, 46: 537–541.
- [37] WRIGHT S, ZHANG L, SUN S, JAHANSHAHI S. Viscosity of a $\text{CaO-MgO-Al}_2\text{O}_3\text{-SiO}_2$ melt containing spinel particles at 1646 K [J]. *Metallurgical and Materials Transactions B*, 2000, 31: 97–104.
- [38] XIAO Wen-bing, YAO Shi-wen, ZHOU Shi-wei, WEI Yong-gang, LI Bo, WANG Hua. Evolution of the structure and viscosity of copper slag during metallization–reduction [J]. *Journal of Alloys and Compounds*, 2022, 903: 163751.
- [39] XU Ji-fang, ZHANG Jie-yu, JIE Chang, LIU Gong-yuan, RUAN Fei. Measuring and modeling of viscosities of selected $\text{CaO-MgO-Al}_2\text{O}_3\text{-SiO}_2$ Slags [J]. *Advanced Materials Research*, 2011, 152/153: 782–790.
- [40] XU Ji-fang, SU Li-juan, CHEN Dong, ZHANG Jie-yu, CHEN Yao. Experimental investigation on viscosity of $\text{CaO-MgO(-Al}_2\text{O}_3\text{)-SiO}_2$ slags and solid-liquid mixtures [J]. *Journal of Iron and Steel Research International*, 2015, 22: 1091–1097.
- [41] ZHANG Tong-sheng, ZHANG Hua-long, DAI Shi-fan, HUANG Dao-yuan, WANG Wan-lin. Variation of viscosity and crystallization properties of synthetic ferronickel waste slag with Al_2O_3 content [J]. *Ceramics International*, 2021, 47(16): 22918–22923.
- [42] SADYKOV S B, KOZHAKHMETOV S M, KVVYATKOVSKIY S A, SADYKOV T S, CHEKIMBAEV A F. Study of properties of artificial slags modeling smelting slags of oxidized cobalt-nickel ores of the Gornostaevskeye deposit [J]. *Kompleksnoe Ispolzovanie Mineralnogo Syrja*, 2015, 1: 59–63. (in Russian)
- [43] Slag Atlas [M]. 2nd ed. Verein Deutscher Eisenhüttenleute, ed. Düsseldorf: Verlag Stahleisen, 1995.
- [44] VANJUKOV A V, ZAJTSEV V J. Mattes and slags of non-ferrous metallurgy [M]. Moscow: Metallurgija, 1969. (in Russian)
- [45] CAI Peng-cheng, LUAN Jun, LIU Jia-heng, LI Chao, YU Zhi-gang, ZHANG Jie-yu, CHOU Kuochih. A modified method for calculating the viscosity of multicomponent slags based on Kriging interpolation [J]. *Ceramics International*, 2022, 48(15): 21803–21811.
- [46] CHEN Zi-wei, WANG Ming-hao, MENG Zhao, WANG Hao, LIU Li-li, WANG Xi-dong. Development of structure-informed artificial neural network for accurately modeling viscosity of multicomponent molten slags [J]. *Ceramics International*, 2021, 47(21): 30691–30701.
- [47] IIDA T, SAKAI H, KITA Y, MURAKAMI K. Equation for estimating viscosities of industrial mold fluxes [J]. *High Temperature Materials and Processes*, 2000, 19(3/4): 153–164.
- [48] MILLS K C, SRIDHAR S. Viscosities of ironmaking and steelmaking slags [J]. *Ironmaking & Steelmaking*, 1999, 26(4): 262–268.
- [49] RIBOUD P V, ROUX Y, LUCAS L D, GAYE H. Improvement of continuous casting powders [J]. *Fachber Huttenprax Metallweiterverarb*, 1981, 19(10): 859–869.
- [50] SEETHARAMAN S, SICHEN Du, ZHANG J Y. The computer-based study of multicomponent slag viscosities [J]. *JOM*, 1999, 51: 38–40.
- [51] SUZUKI M, JAK E. Quasi-chemical viscosity model for fully liquid slag in the $\text{Al}_2\text{O}_3\text{-CaO-MgO-SiO}_2$ system. Part II: Evaluation of slag viscosities [J]. *Metallurgical and Materials Transactions B*, 2013, 44: 1451–1465.
- [52] URBAIN G. Viscosity estimation of slags [J]. *Steel Research*, 1987, 58: 111–116.
- [53] van DYK J C, WAANDERS F B, BENSON S A, LAUMB M L, HACK K. Viscosity predictions of the slag composition of gasified coal, utilizing FactSage equilibrium modelling [J]. *Fuel*, 2009, 88: 67–74.
- [54] YAN Zhi-ming, REDDY R G, LV Xue-wei, PANG Zheng-de, BAI Chen-guang. Viscosity of iron oxide aluminosilicate melts [J]. *Metallurgical and Materials Transactions B*, 2019, 50: 251–261.
- [55] ALTOMARE A, CORRIERO N, CUOCCI C, FALCICCHIO A, MOLITERNI A, RIZZI R. QUALX2.0: A qualitative phase analysis software using the freely available database POW_COD [J]. *Journal of Applied Crystallography*, 2015, 48: 598–603.
- [56] ASTM E112–13. Standard Test Methods for Determining Average Grain Size. ASTM International [S]. <https://www.astm.org/e0112-13.html>. Accessed 25 Jun 2021.
- [57] MathWorks total academic headcount – Full suite [M]. The MathWorks, Inc. 1994–2020.
- [58] ARKHANGELSKY I V, DUNAEV A V, MAKARENKO I V, TIKHONOV N A, BELYAEV S S, TARASOV A V. Non-isothermal kinetic methods. Workbook and laboratory manual non-isothermal kinetic methods. Workbook and laboratory manual [M/OL]. Edition Open Access, 2013. <http://edition-open-access.de/media/textbooks/1/Textbooks1.pdf>. Accessed 23 Aug 2022.
- [59] LINCHEVSKIY B V. Technique of the metallurgical experiment [M]. Moscow: Metallurgija, 1979. (in Russian)
- [60] ARSENTYEV P P, JAKOVLEV V V, KRASHENINNIKOV M G, PRONIN L A, FILIPPOV E S. Physico-chemical methods for studying metallurgical processes [M]. Moscow: Metallurgija, 1988. (in Russian)
- [61] SHTENGELMEJER S V. Electromagnetic vibrating viscometer [J]. *Zavodskaja Laboratorija*, 1964, 2: 238–239. (in Russian)
- [62] SHTENGELMEJER S V. Calibration of vibrating viscometers [J]. *Zavodskaja Laboratorija*, 1973, 39(2): 239–240. (in Russian)
- [63] SHTENGELMEJER S V, PRUSOV V A, BOCHEGOV V A. Improving the method for measuring viscosity with a vibrating viscometer [J]. *Zavodskaja Laboratorija*, 1985, 51(9): 56–57. (in Russian)
- [64] WEYMANN H D. On the hole theory of viscosity, compressibility, and expansivity of liquids [J]. *Kolloid-*

Zeitschrift und Zeitschrift für Polymere, 1962, 181:
131–137.

[65] GUDIMA N V, KARASEV J A, KISTJAKOVSKIJ B B,

KOLKER P E, RAVDANIS B I. Technological calculations
in non-ferrous metals metallurgy: Textbook [M]. Moscow:
Metallurgija, 1977. (in Russian)

氧化镍和硫化铜矿联合熔炼炉渣的黏度

Alexander KLYUSHNIKOV¹, Svetlana SERGEEVA¹, Roza GULYAEVA¹,
Alexander VUSIKHIS¹, Lyudmila UDOEVA², Stanislav TYUSHNYAKOV¹

1. Laboratory of Non-Ferrous Metals Pyrometallurgy, Department of Non-Ferrous Metals,
Institute of Metallurgy of the Ural Branch of the Russian Academy of Sciences,
101, Amundsen Street, Yekaterinburg 620016, Russia;
2. Laboratory of Rare Refractory Metals, Department of Non-Ferrous Metals,
Institute of Metallurgy of the Ural Branch of the Russian Academy of Sciences,
101, Amundsen Street, Yekaterinburg 620016, Russia

摘要: 测定氧化镍和硫化铜矿联合熔炼炉渣的黏度。制备的模拟炉渣与实际炉渣的成分和结构相似, 并限制研究的炉渣的成分范围, 含铁炉渣的成分(质量分数)为: 8.9% CaO、11.8% MgO、12.5% Al₂O₃、47.4% SiO₂、13.3% FeO 和 5.0% Fe₂O₃; 无铁炉渣是将含铁炉渣中的氧化铁去除得到, 其成分(质量分数)为: 12.5% CaO、16.0% MgO、9.4% Al₂O₃ 和 58.3% SiO₂。由振动法测试的含铁炉渣(1550~1300 °C)和无铁炉渣(1550~1400 °C)的黏度实验值分别为 0.31~2.33 Pa·s 和 1.28~4.55 Pa·s。由 Kalmanovitch–Frank 模型预测的含铁炉渣的黏度值与实验值存在偏差。通过 Weimann–Frenkel–Urbain 方程对实验数据进行回归分析, 提出可预测所考虑温度范围内的初级炉渣黏度的原始经验模型。当碱度从 0.7(含铁炉渣)降低到 0.6(无铁炉渣), 黏性流动活化能从 204 kJ/mol 增加到 236 kJ/mol。为了保持最佳炉渣黏度, 氧化镍和硫化铜矿联合冶炼的温度应不低于 1400 °C。

关键词: 炉渣; 黏度; 振动式黏度计; Kalmanovitch–Frank 模型; Weimann–Frenkel–Urbain 方程; 氧化镍矿; 硫化铜矿; 造钼熔炼

(Edited by Bing YANG)